CHAPTER 6 SYNTHESIS AND CHARACTERIZATION OF PMMA/ HAPAG COATING ON TI6AL4V SUBSTRATE

This chapter includes the investigation of the properties and potential applications of a novel composite coating made of poly (methyl methacrylate) (PMMA) and silver-doped hydroxyapatite (HAPAg) derived from waste eggshells and dip-coated onto Ti6Al4V substrates. Silver-doped hydroxyapatite nanoparticles are deposited within a PMMA matrix to form the PMMA/HAPAg composite coating, which has antibacterial and osteoconductive properties. The contact angle and total surface free energy (SFE) were examined. SEM was used to examine the surface morphology of the defective zones, and ICPMS, FTIR, and XRD were used to determine the elemental composition of the synthesized materials. Atomic force microscopy (AFM) measures the surface roughness, root mean square roughness, roughness profile, skewness, and kurtosis of coated materials. Finally, the findings are evaluated and debated.

6.1 Results and discussion

The synthesis of silver-doped eggshell-derived HAp with 0.2 wt% Ag in HAp was done, and the obtained powder (particle size approximately 18 μm) was reinforced in PMMA with 10, 15 and 20 wt%. The prepared sol was used for dip coating, and the wettability, morphology and topography were analyzed. The elemental analysis of the synthesized silver-doped HAp using ICPMS is given in **Table 6.1**. It reflects the presence of the precursors with a Ca/P (molar ratio) of 1.521.

Table 6.1. Elemental Analysis of synthesized eggshell-derived silver-doped HAp.

Sample	Ca (wt%)	P (wt%)	Ag (wt%)	Ca/P (Molar ratio)
Silver-Doped HAp	30.67± 01	15.65 ± 01	0.142 ± 0.05	1.521

6.1.1 FTIR Analysis

The FTIR spectra of PMMA/H0, PMMA/H10, PMMA/H15 and PMMA/H20 coating samples are shown in **Fig. 6.1.** The intense vibration peak at 1723 cm^{-1} shows the presence of stretching vibration of ester carbonyl (C-O) group in the coating material [204]. The decrease in the intensity of PMMA peaks with an increase in HAp reinforcement, reflects the presence of HAp in PMMA. The CH_2 vibrational peaks are observed adjoining 749.2, 840.3 and 985.9 cm^{-1}.

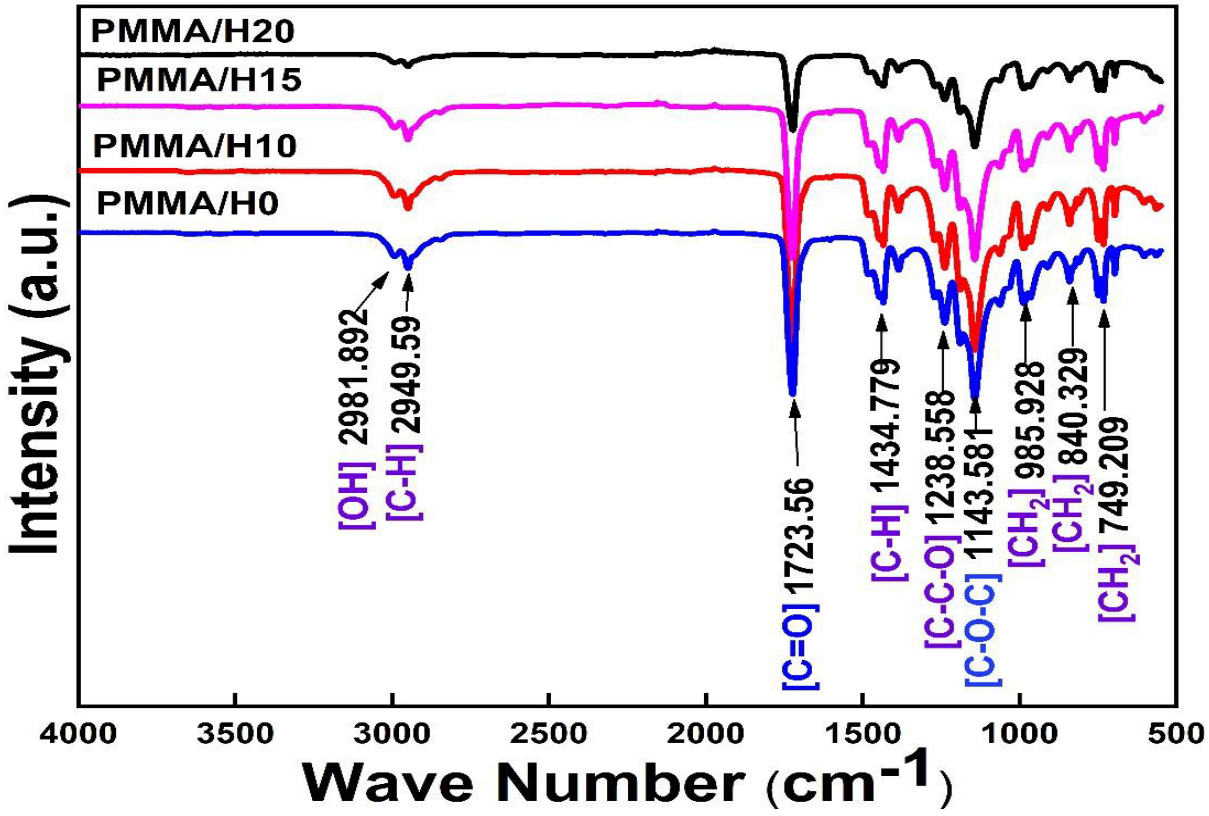

Fig. 6.1. FTIR spectrum of PMMA/H0, PMMA/H10, PMMA/H15 and PMMA/H20 coating.

An asymmetric stretching of the C-O-C functional group appeared at 1143.58 cm^{-1}. Stretching peaks at 1238 cm^{-1} attributed to C-C-O vibration in the methyl carbonyl

group. However, vibrational peaks at 1434 and 2949 cm^{-1} correspond to the C-H bonding deformation. The variation in the intensity of peaks varies with the reinforcement of HAPAg in PMMA. The FTIR spectra obtained are in consistent with the previous available research [125,205].

6.1.2 XRD Analysis

The X-ray diffractogram of the hydroxyapatite powder obtained from eggshells, which has been manufactured with the addition of silver is illustrated in **Fig. 6.2**. Validating the peaks using the standard JCPDS No: 01-074-0545. The plane (2 1 1) located at a 2θ position of 31.760 exhibits 100% intensity of HAp with a d-spacing of 2.8 Å. Similarly, the plane (3 0 0) at a 2θ position of 32.90 exhibits 60.9% intensity with a d-spacing of 2.7 Å.

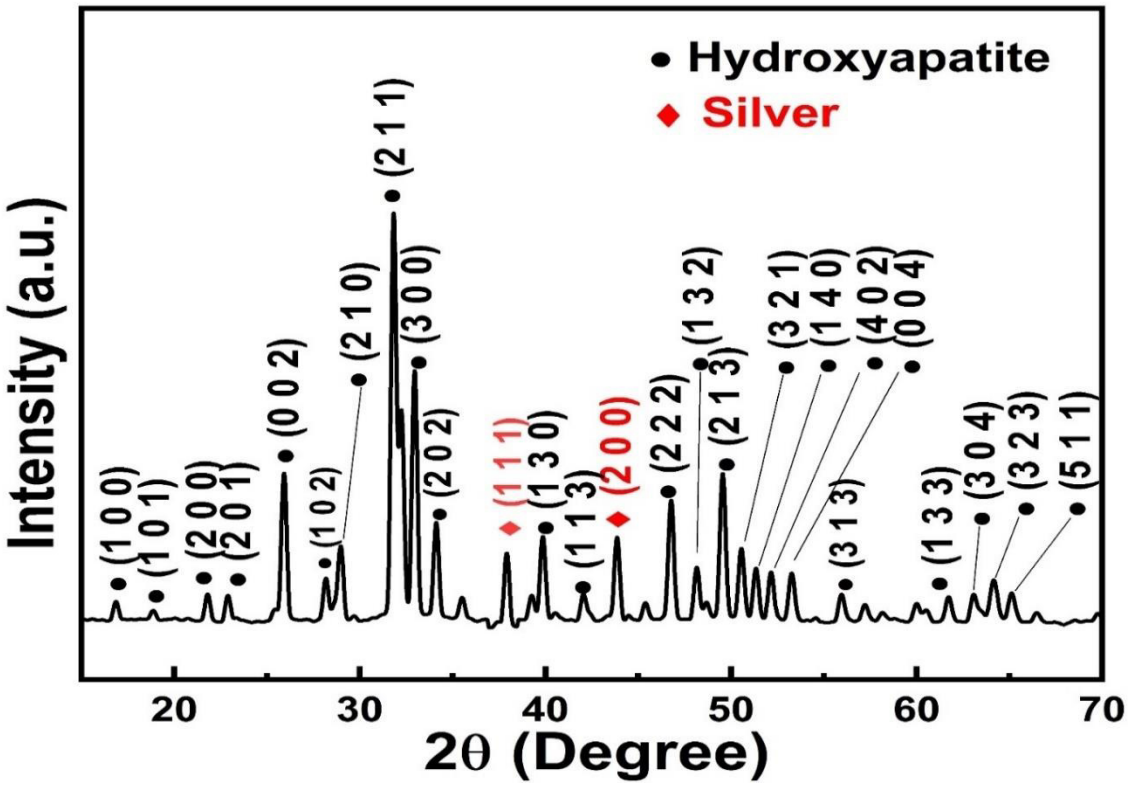

Fig. 6.2. XRD spectra of Silver-doped eggshell-derived hydroxyapatite.

The product exhibits a significant degree of phase purity and chemical synthesis. The incorporation of silver during the synthesis of HAp has a negligible impact on the compound formation and functions to replenish the vacant interplanar gaps.

Moreover, the marginal rise in the highest level of strength indicates the unique impact of silver nitrate doping when employed as a suitable base for evaluating the antibacterial characteristics of the modified HAP. The low concentration of silver ions in the HAp powder suggests that monovalent silver ions can replace calcium ions without affecting the crystal structure of HAP [189]. Kostov-Kytin et al. [206] had comparable outcomes on HAp and β-TCP.

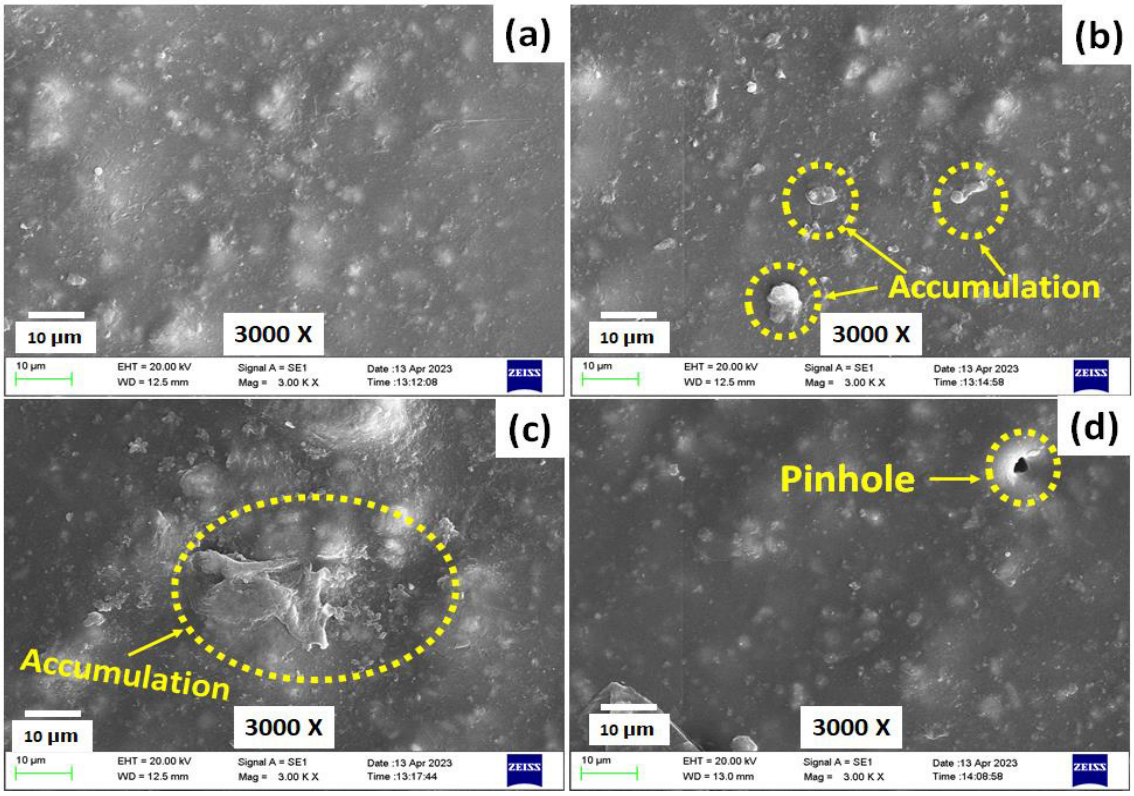

Fig. 6.3. SEM images of the Dip coated samples at 3000x magnification.

The SEM images at the micro-defected zones of dip-coated surface with 3000 X magnification are shown in **Fig. 6.3 (a-d)**. The images highlight the irregularities and uneven surface morphology that occurred near the bottom edge during the coating of Ti6Al4V with HAp-reinforced PMMA. As observed, the uniform coating with slight

deformation and accumulation near the bottom edge of the coated surface occurred due to the capillary action during the vertical dip coating process [207]. It is recommended to conserve geometrical tolerance in the substrate to attain defect free coating. The accumulation of reinforced silver-doped HAp in the PMMA sol solution was observed in **Fig. 6.3 (b and c)**. The accumulation occurred due to the density difference in the suspension liquid of PMMA/H10 and PMMA/H15. The magnitude of theoretical density (ρ_T) calculated using rules of mixture for PMMA/H0, PMMA/H10, PMMA/H15 and PMMA/H20 are 1.19 g/cm^3, 1.389 g/cm^3, 1.48985 g/cm^3 and 1.5898 g/cm^3, respectively is tabulated in **Table 6.2**. The increase in density is linearly governed by the decrease in PMMA concentration with increase in HAPAg in composite formation. The accumulation occurs at the bottom edge of the coated samples. Also, a small pinhole defect was observed (**Fig. 6.3 (d)**) in the PMMA/H20 sample that could be due to improper wetting, drying, air entrapment or high surface tension that leads to the uneven spreading of coating on the Ti6Al4V substrate. Multiple laboratory trials were performed to optimize the coating material and the defects were reduced by performing the coating in a controlled environment and preserving the coated samples in a vacuum at least for 24 hours. Therefore, it can be interpreted that, the dip coating defects are controllable and can be reduced easily by systematic monitoring and parametrical modifications [208].

6.1.3 Adhesion Strength

The strength of coating deposition was analysed to check its adhesion with the substrate material by calculating the critical nomal load for various compositions. **Figure 6.4** illustrates a macrograph alongside 2D and 3D topography, showcasing the scratch behavior resulting from the linear movement of a spherical indenter (200 μm diameter) on the coated surface, ranging progressively from 0 to 25 N of normal

loading. The critical normal load (L_c) was determined by averaging three tests per sample. The average Lc magnitudes for PMMA/H0, PMMA/H10, PMMA/H15, and PMMA/H20 were found to be 0.967 ± 0.249 N, 1.1 ± 0.245 N, 17.33 ± 1.25 N, and 20.33 ± 6.59 N, respectively.

Table 6.2. Theoretical density, coating thickness and critical normal load of coating sample.

Sample	Theoretical Mass Density (ρ), (g/cm^3)	Coating Thickness (t), (μm)	Critical Normal Load (Lc), (10^{-1} N)
PMMA/H0	1.1900 ± 0.001	73.25 ± 10.39	09.67 ± 2.49
PMMA/H10	1.3899 ± 0.001	77.77 ± 08.95	11.00 ± 2.45
PMMA/H15	1.4898 ± 0.001	87.42 ± 10.28	17.33 ± 1.25
PMMA/H20	1.5898 ± 0.001	89.32 ± 10.28	20.33 ± 6.59

However, the magnitude of Lc at a constant area reflects the low adhesion strength of dip-coated samples [144] compared to other coating methods for PMMA/ hydroxyapatite deposition [209,210]. Notably, the average Lc increases with the reinforcement of HAPAg in PMMA, indicating the comparatively enhanced adhesion strength of the PMMA/H20 coating on Ti6Al4V. This enhancement is attributed to increased chemical adhesion between the organic PMMA and inorganic HAPAg, thereby potentially strengthening the overall composite. Furthermore, the addition of HAPAg to PMMA significantly increases the mass density and brittleness of the composite coating. The scratch behavior depicted in **Fig. 6.4 (a)** exhibits evident plastic deformation, along with raised sides and burrs at the edges. Conversely, the coatings reinforced with HAPAg in PMMA (**Fig. 6.4 (b-d)**) display plugging and brittle failure with the progressive increase in normal load and scratching velocity. Moreover, a slight increase in coating thickness from 73.25 μm (PMMA/H0) to 89.32 μm (PMMA/H20) may contribute to the heightened brittle failure in adhesion strength. Additionally, as the coating demonstrates brittle characteristics with HAPAg

reinforcement, it likely possesses high hardness [211] with rise in concentration. This behavior aligns with observations in the current analysis, where coating spallation occurred in the form of brittle cracks and delamination as the normal load increased during scratching. Sudden flaking was observed at stylus velocity of 0.5 mm/s for PMMA/H0 and PMMA/H10, while the similar detachment was noted at 1.0 mm/s for PMMA/H15 and PMMA/H20 coatings during the scratch test. These occurrences resulted in weakened coating adhesion and interlocking between the coating and the substrate working at higher speeds.

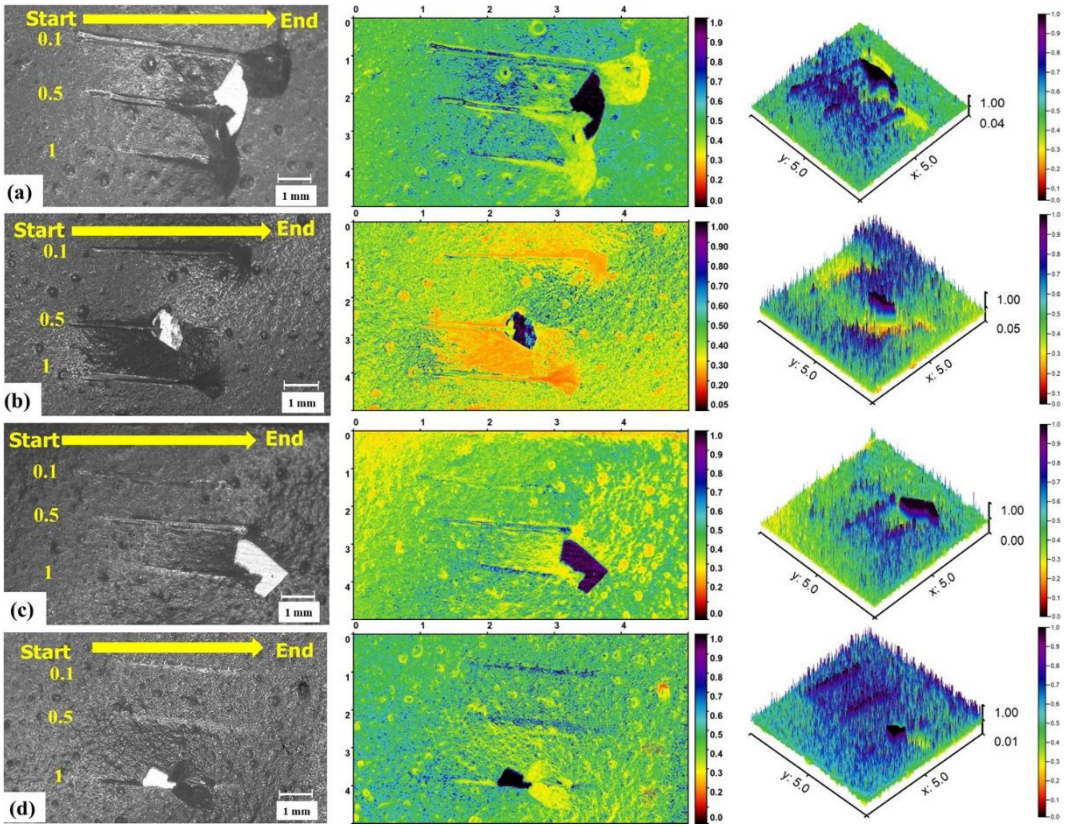

Fig. 6.4. Macrograph, 2D and 3D topography of scratch test images on (a) PMMA/H0, (b) PMMA/H10, (c) PMMA/H15, and (d) PMMA/H20 coated samples.

The **Fig. 6.5 (a-d)** shows the cross-sectional micrograph of the coated samples to determine the coating thickness. The average thickness (**Fig. 6.5 (e)**) of the coated samples were measured using ImageJ software with fifteen readings per sample. The thickness values of PMMA/H0, PMMA/H10, PMMA/H15 and PMMA/H20 on

Ti6Al4V substrate were 73.25 ± 10.39 µm, 77.77 ± 8.95 µm, 87.42 ± 10.28 µm and 89.32 ± 13.39 µm, respectively.

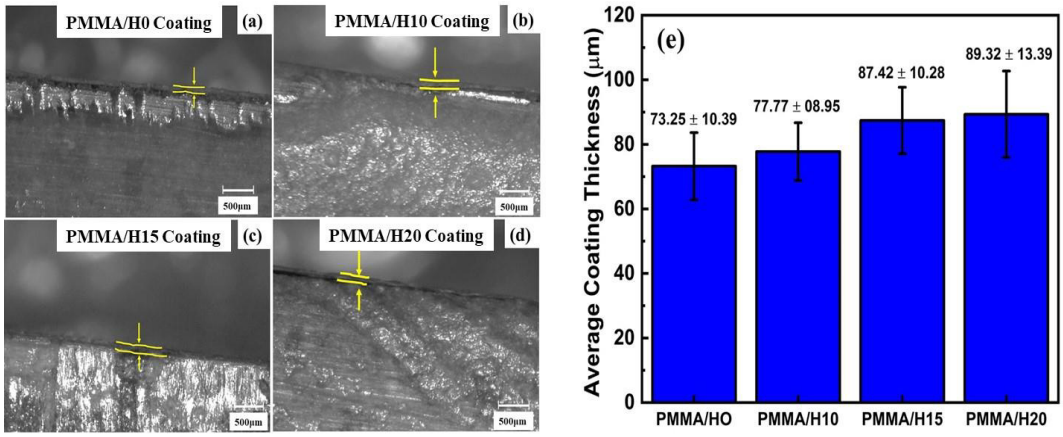

Fig. 6.5. Micrograph representing coating thickness of (a) PMMA/H0, (b) PMMA/H10, (c) PMMA/H15 and (d) PMMA/H20 on Ti6Al4V substrate, and (e) average coating thickness.

As observed, the coating thickness increases with the increase in HAPAg reinforcement in PMMA. The thickness also effects the adhesion strength between the coating and the substrate. Moreover, the obtained thickness is an acceptable deposition for biomimic coating on metallic implant and it promotes the osseointegration and reduces stress shielding effect of the metallic implant [212].

6.1.4 Wettability Analysis

The wettability of the coated sample was determined through the CA measurement with an average of five sessile droplets of distilled water and Diiodomethane on the surface of the coating [213]. The results obtained are shown in **Fig. 6.6.** As observed, the CA on the surface of the undoped Ti6Al4V sample was $60.86^0 \pm 0.98^0$ with the water droplet and $47.52^0 \pm 0.85^0$ with the Diiodomethane droplet. The average ± SD values of the CA for PMMA/H0, PMMA/H10, PMMA/H15 and PMMA/H20 coating on Ti6Al4V substrate using water droplet were $75.27^0 \pm 1.69^0$, $74.83^0 \pm 0.99^0$, $70.48^0 \pm 0.95^0$ and $70^0 \pm 1.44^0$, respectively and for Diiodomethane sessile droplet the CA values were $55.64^0 \pm 1.91^0$, $53.12^0 \pm 0.87^0$, $50.64^0 \pm 0.93^0$ and $49.65^0 \pm 1.05^0$,

respectively. The surface wettability (hydrophobicity or hydrophilicity) of the material is liquid dependent, i.e., it alters its contact properties as per the interaction between the solid-liquid interface. The CA obtained using water droplets for PMMA/HAp coated samples was comparatively higher than that of Diiodomethane for all the compositions. However, a slight decrease in CA was observed with the increase in Silver-doped HAp in PMMA. The increase in hydrophilicity characteristic was due to the presence of the –OH functional group in HAp [214]. Also, Ag-doped HAp with PMMA promotes antibacterial characteristics with improved biocompatibility and adhesion in coating applications [119]. The low CA promotes high surface coverage and the highest level of cell attachment [161]. However, a 7.03% (± 5^0) change in hydrophilicity was observed between PMMA/H0 and PMMA/H20, revealing the consistent SFE of the coated samples till 20 wt% of HAPAg in PMMA.

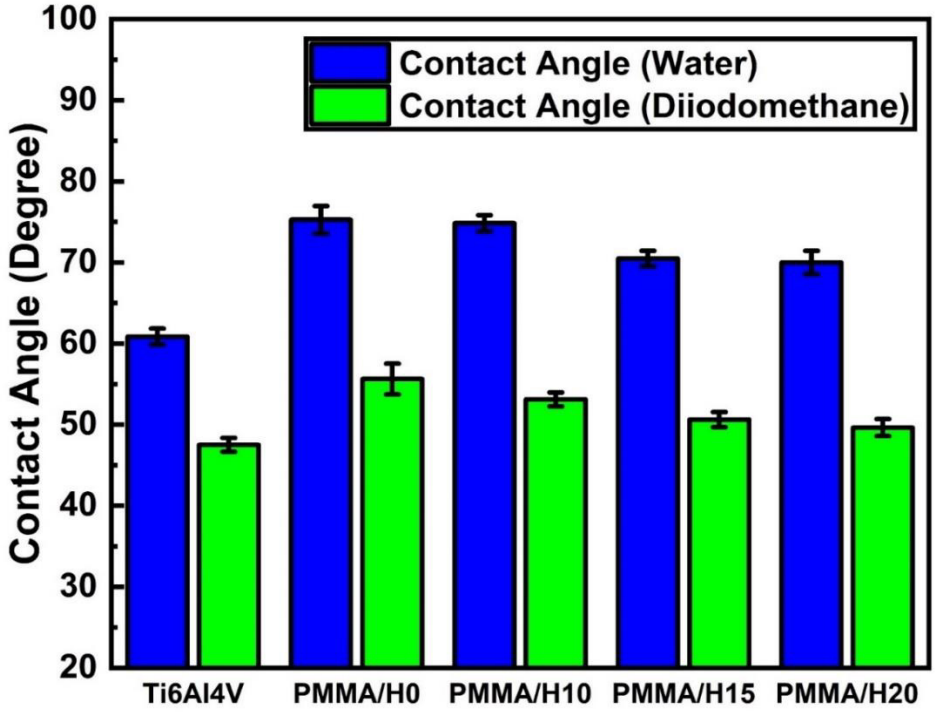

Fig. 6.6. Contact angle measurement on coated and uncoated samples using water and Diiodomethane droplet.

The average values of CA were used to determine the SFE of the coated and uncoated samples using Owens Wendt Equation (equation 1 & 2). The magnitude of the

dispersive component, polar component and total SFE of the coated and uncoated samples are plotted in **Fig. 6.7.** As observed, the total SFE of the coated samples was slightly less than the uncoated sample, which implies that the surface of uncoated sample has comparatively higher surface adhesion to liquid. The total SFE of the uncoated sample as computed from the CA values, was 49.15 ± 01 mJ/m^2 (E_p = 13.51 ± 01 mJ/m^2 and E_d = 35.65 ± 01 mJ/m^2). Similarly, the computed values of total SFE of coated samples PMMA/H0, PMMA/H10, PMMA/H15, PMMA/H20 are 38.63 ± 01 mJ/m^2, 39.82 ± 01 mJ/m^2, 42.87 ± 01 mJ/m^2 and 43.47 ± 01 mJ/m^2, respectively. The error of ± 1 mJ/m^2 was considered in evaluating SFE by empirical method [146] and direct reading from the CA measurement machine. As observed, the SFE of the coated samples is significantly lower than that of the uncoated sample (**Fig. 6.7**).

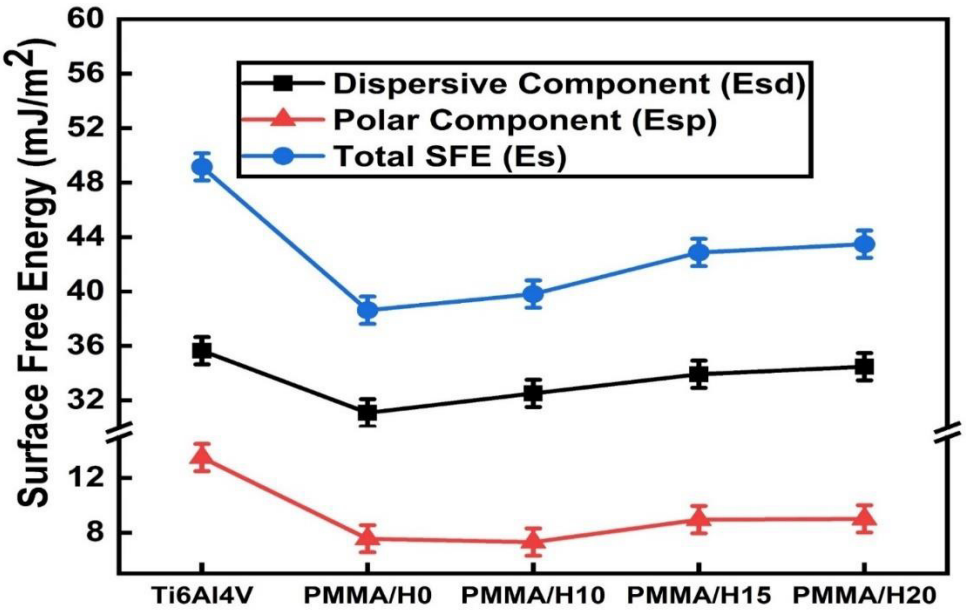

Fig. 6.7. Polar component, dispersive component and total SFE of the coated and uncoated sample.

The low magnitude of SFE improves the antifouling application of the coating as reported by Zhang, H et al. [215]. Also, the relation between the adhesion strength and SFE was reported by Yamauchi, K et al. [216] and Ghanbari & Attar [217]. The adhesion of coating depends on the chemical bond strength at the interface of coating

and the substrate [218]. Consequently, the marginal increase in SFE for coated samples from 38.63 ± 01 mJ/m^2 (for PMMA/H0) to 43.47 ± 01 mJ/m^2 ((for PMMA/H20)) with increase in HAPAg content in PMMA was interpreted for higher adhesion strength between the coating and the substrate. Also, a preclinical study by Buser et al. [219] showed that the implants with a hydrophilic surface accelerated the minipig maxillary osseointegration process (49.30 vs. 29.42% at 2 weeks and 81.91 vs. 66.57% at 4 weeks) compared to hydrophobic implants. Similarly, a clinical study by Lang et al. [220] also showed that implants with hydrophilic surfaces enhance osseointegration compared with hydrophobic surfaces after 28 days of implant placement (48.3% vs. 34.2%).

6.1.5 Topographical Analysis

The 3D topography of the surface of the coated sample taken on 40 µm x 40 µm bed size with pie mode, 30^0 viewpoint adjustment and optimized Z-coloration using Nova Px 3.4 software following ASME B46 standard is shown in **Fig. 6.8 (a-d)**. The results show a high surface finish with an average surface roughness (Sa) of 0.062 µm and root mean square roughness (Sq) of 0.0798 µm in 3D for PMMA/H0 coating on Ti6Al4V. The surface roughness shows a slight increase with the inclusion of silver-doped HAp in PMMA.

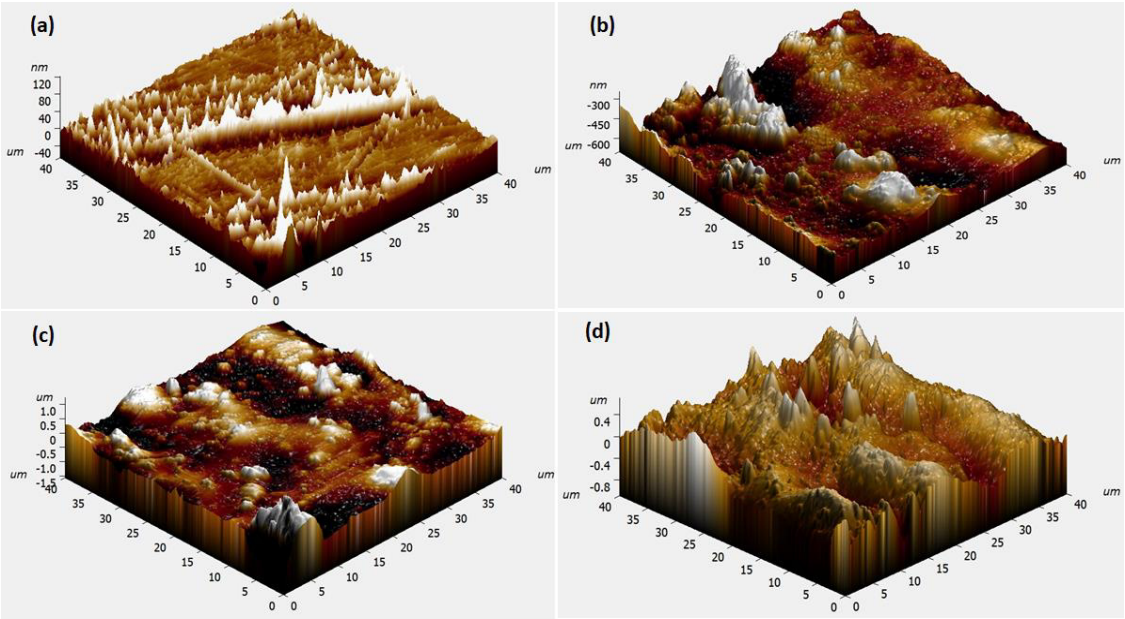

Fig. 6.8. Three-dimensional topography of (a) PMMA/H0, (b) PMMA/H10, (c) PMMA/H15, and (d) PMMA/H20 sample using AFM.

However, the average surface roughness (Sa or Ra) of coatings with PMMA/H10, PMMA/H15 AND PMMA/H20 composition was 0.09 µm, 0.102 µm and 0.167 µm, and the root mean square roughness (Sq) were 0.127 µm, 0.157 µm and 0.210 µm, respectively. **Figure. 6.8 (a-d)** shows the 3D peaks and valleys in the nano roughness range. The high surface finish is attributed to the polymeric outer layer of PMMA coating.

Table 6.3. Skewness and Kurtosis value of coated sample in 2D and 3D topography.

Sample	2D		3D	
	Skewness (R_{sk})	**Kurtosis (R_{ku})**	**Skewness (S_{sk})**	**Kurtosis (S_{ku})**
PMMA/H0	2.017	9.210	1.334	11.771
PMMA/H10	1.231	3.743	0.622	5.656
PMMA/H15	0.556	2.638	0.187	14.772
PMMA/H20	0.926	3.086	-0.194	3.2

The **Fig. 6.9** shows the 2D topography of the PMMA/H0, PMMA/H10, PMMA/H15 AND PMMA/H20 coated samples taken on a 40 µm x 40 µm bed size. The 30 µm roughness profile taken diagonally on the 2D topography image was plotted separately

as shown in **Fig. 6.10.** The results show the high surface finish with the 2D average surface roughness (Ra) of 0.005 µm and root mean square roughness (Rq) of 0.009 µm in 2D for PMMA/H0 coating on Ti6Al4V. The surface roughness shows a slight increase with the inclusion of silver-doped HAp in PMMA. However, the average surface roughness (Ra) of coatings with PMMA/H10, PMMA/H15 AND PMMA/H20 composition was 0.055 µm, 0.06 µm and 0.14 µm, and the root mean square roughness (Rq) were 0.069 µm, 0.074 µm and 0.171µm, respectively.

The shape factor analysis of the coated surfaces was analyzed by determining the skewness (R_{sk} and S_{sk}) and kurtosis (R_{ku} and S_{ku}) values of coated samples using 2D and 3D topography. The skewness determines the degree and direction of asymmetric distribution in the sample's surface features that occurred during coating [221]. In contrast, the kurtosis data signifies the peakiness and flatness of the overall surface texture [222]. The magnitude of skewness and kurtosis tabulated in **Table 6.3** were obtained using AFM at 40 x 40 µm evaluation area. It helps to quantify the deviation of the surface from a Gaussian (normal) distribution [223]. As observed, PMMA/H0 shows 2.017 µm skewness in 2D and 1.334 µm in 3D. However, the kurtosis values show 9.21 µm in 2D and 11.771 µm in 3D. The 54.09 % and 66.49 % decrease in 2D skewness and kurtosis, respectively, whereas 72.81 % and 85.54 % decrease in 3D skewness and kurtosis, respectively, was observed between PMMA/H0 and PMMA/H20.

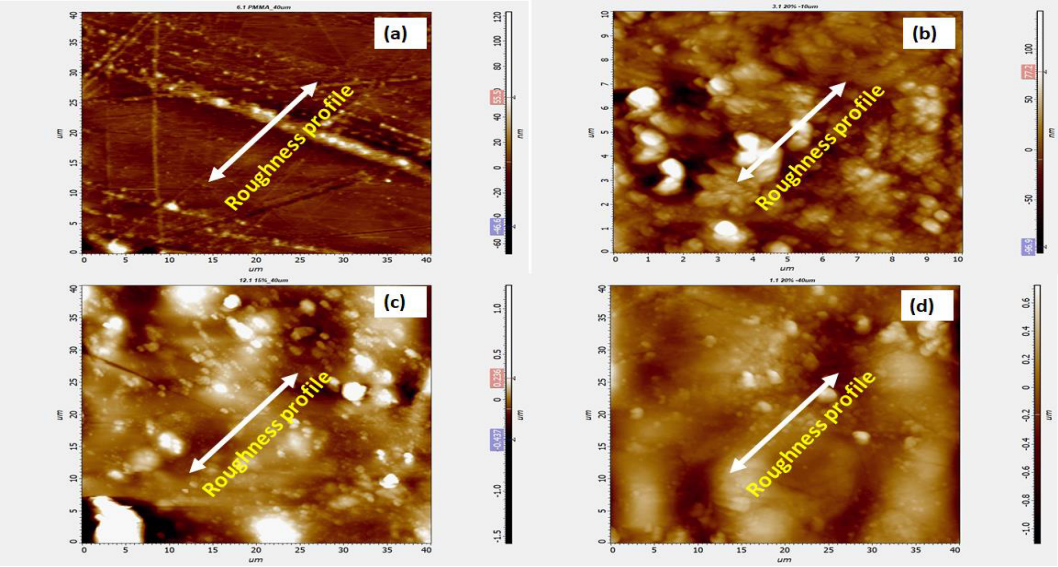

Fig. 6.9. Two-dimensional topography of (a) PMMA/H0, (b) PMMA/H10, (c) PMMA/H15, and (d) PMMA/H20 sample using AFM.

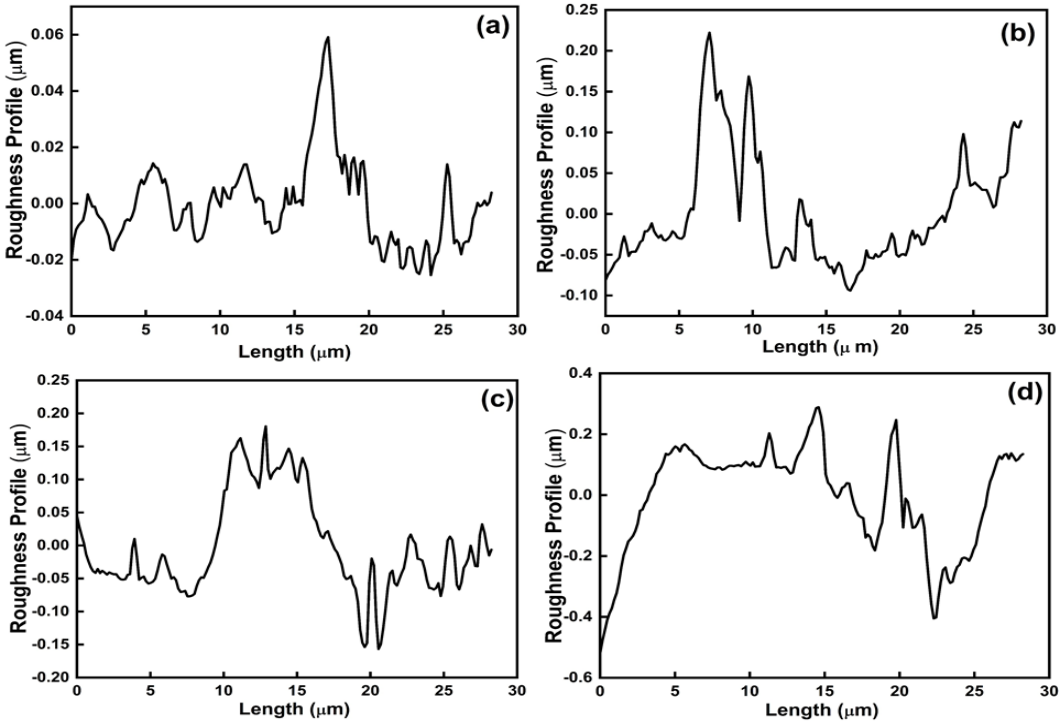

Fig. 6.10. Two-dimensional roughness profile of (a) PMMA/H0, (b) PMMA/H10, (c) PMMA/H15, and (d) PMMA/H20 sample using AFM.

6.1.6 Well Diffusion Analysis

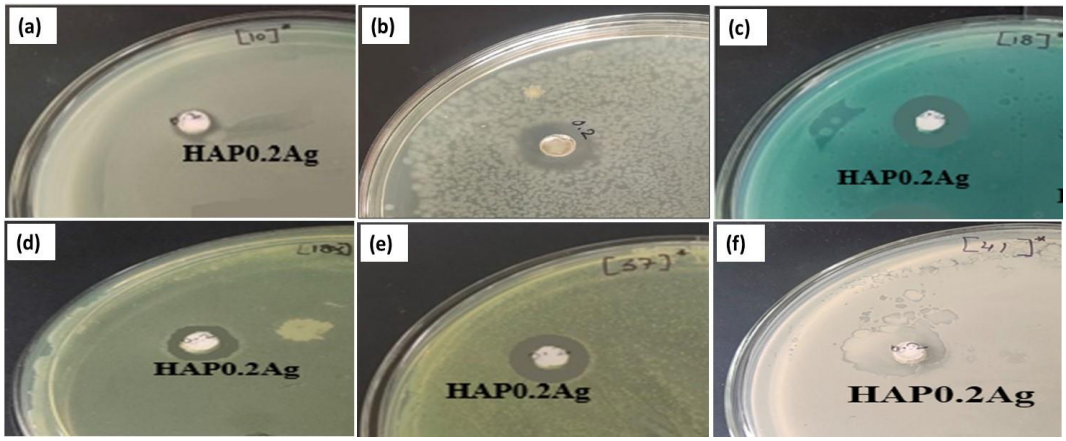

Fig. 6.11. Pictorial representation of Diameter of Inhibition of 0.2 wt% silver-doped hydroxyapatite (a) S. epidermidis, (b) P. aeruginosa, (c) E. coli, (d) E. coli DH5a, (e) S. aureus, and (f) B. subtilis bacterial culture after 24 h of incubation.

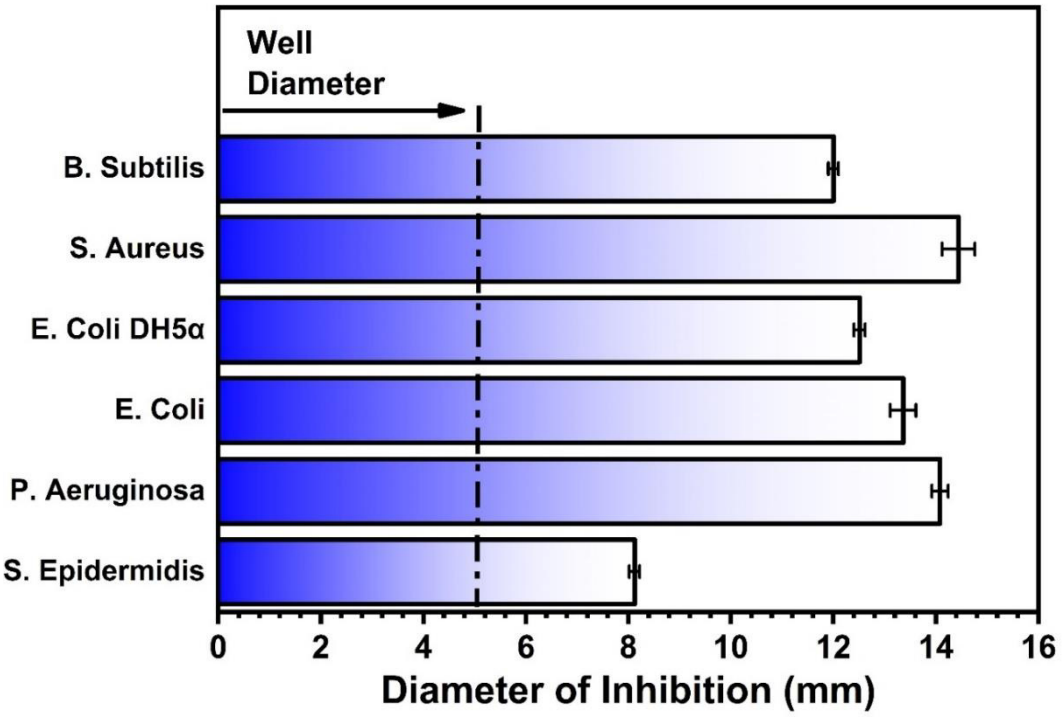

Fig. 6.12. Diameter of Inhibition of 0.2 wt% silver-doped hydroxyapatite under different microorganisms.

The antibacterial efficacy of the reinforced particulate examined before the fabrication of composite was performed using well diffusion method. The pictorial representation to measure the diameter of inhibition of 0.2 wt% silver-doped hydroxyapatite powder was examined for several microorganisms as shown in **Fig. 6.11**. The obtained results

revealed that the HAP0.2Ag powder shows effective antibacterial nature under all bacterial strains and thus concludes its application in antibacterial coating and grafting. The DoI under *S. epidermidis, P. Aeruginosa, E. Coli, E. Coli DH5α, S. aureus* and *B. subtilis* strains were 08.12 ± 0.10, 14.08 ± 0.16, 13.36 ± 0.25, 12.51 ± 0.11, 14.44 ± 0.32 and 12.00 ± 0.10 mm, respectively. The same is highlighted in **Fig. 6.12.** Amalgamation of PMMA and HAPAg coating on Ti6Al4V substrate provides high strength, biocompatibility and antibacterial outputs that are highly beneficial in biomedical applications.